EFFECTS OF SURFACE ORIENTATION ON WALL HEAT FLUX PARTITIONING DURING NUCLEATE POOL BOILING OF SATURATED WATER AT ATMOSPHERIC PRESSURE

Satbyoul Jung and Hyungdae Kim*
Department of Nuclear Engineering, Kyung Hee University, Yongin, Republic of Korea
Corresponding Address
hdkims@khu.ac.kr

ABSTRACT

Orientation of the wall exerts a strong influence on the bubble-scale parameters during nucleate boiling and the resulting wall heat flux. A number of mechanistic models have been developed for the prediction of wall heat flux and partitioning in nucleate boiling. The mechanistic model by Kurul and Podowski (usually called as the RPI model), is widely employed in two-phase computational fluid dynamic and thermal-hydraulics codes for nuclear reactor system analysis. However, the RPI model was not developed with taking effects of surface orientation on the bubble-scale parameters and wall heat flux of nucleate boiling into account. This study aims at experimentally examining effects of the surface orientation on the bubble-scale parameters and wall heat flux of nucleate boiling and improving the prediction accuracy of the RPI wall heat flux partitioning model. In this study, nucleate boiling experiments of saturated water under atmospheric condition were conducted on a wall with a constant surface temperature of 107.5 °C. Orientation of the boiling wall changed from 0 (upward-facing horizontal) to 30, 60, 90° (vertical). A unique optical setup integrating infrared thermometry, total reflection, and shadowgraph techniques in the present study permitted to simultaneously acquire quantitative data on all the bubble-scale parameters related with the sub-models, including nucleation site density, bubble departure diameter and frequency, bubble wait time. The bubble parameters and total wall heat flux obtained from experiment and the RPI model are compared with regard to surface orientation. There was a big difference in them between measured data and prediction data by RPI model. The main cause of that was the effect of bubble merging; the effect of bubble sliding was negligible. The evaporation was a dominant contributor for heat flux with surface orientation of 0, 30, 60, 90°

KEYWORDS
Atmospheric pressure, Nucleate pool boiling, Surface orientation, Wall heat flux partitioning

1. INTRODUCTION

Nucleate boiling in LWRs may occur in several thermal-hydraulic components with different wall orientations, such as the cylindrical fuel rods vertically mounted in the reactor vessel, the curved bottom surface of the reactor vessel for IVR-ERVC and various types of heat exchangers. Nucleate boiling heat transfer is closely associated with the dynamics of bubble growth and departure on the heated surface, and the dynamic behavior of bubbles is influenced by the gravitational force. Therefore, the surface orientation can play an important role in nucleate boiling heat transfer.

There have been a number of studies to investigate the surface orientation effects on boiling heat transfer. Several studies reported that the nucleate boiling heat transfer performance increases at a given wall

temperature as the surface orientation rotates from upward-facing horizontal to vertical [1-2]. Nishikawa et al.[3] reported that there is a significant effect of surface orientation on heat transfer coefficient in low heat flux region, while no remarkable effect in the high heat flux region for water on copper plate, when the surface orientation is inclined from 0° (upward-facing horizontal) to 175°. Chang and You [4], examining the pool boiling behavior of saturated FC-72 on a plain cooper surface, observed that the heat transfer rate increase 0°(upward-facing horizontal) to 90° and then diminish dramatically from 90° to 180° in nucleate boiling regime.

Recently, there are efforts to predict the nucleate boiling heat transfer in nuclear reactor using Computational Fluid Dynamics (CFD) code. The commercial CFD codes include the wall heat flux partitioning model to predict the nucleate boiling heat transfer. Rensselaer Polytechnic Institute (RPI) model of Kurul and Podowski [5] is widely used in commercial CFD code. However, the RPI wall heat flux partitioning model do not include the dependency on surface orientation, even though the boiling heat transfer mechanisms could be strongly distorted by the surface orientation (i.e., the dynamic of the bubble on the heated wall such as bubble sliding and merging).

In this study, we experimentally examine the effects of surface orientation on wall heat flux partitioning during saturated pool boiling at atmospheric pressure. The measured data for bubble parameters and total wall heat flux are compared with RPI model with regard to surface orientation. We examine the reason for differences between measured data in present study and prediction by RPI model and discuss the physical mechanism leading to change of the heat transfer performance.

2. REVIEW OF RPI WALL HEAT FLUX PARTITIONING MODEL

The RPI wall heat flux partitioning model is reviewed to examine the model and deduce the needs of consideration of the wall orientation. In the RPI model, the total wall heat flux from a heated wall to the fluid is partitioned into three heat fluxes: evaporative, quenching, and convective:

$$q_w'' = q_e'' + q_q'' + q_c'' \tag{1}$$

A conceptual description of the model is shown in Fig. 1.

The evaporative heat flux, q_e'', is the latent heat flux required to form the bubbles and can be expressed as

$$q_e'' = N'' f\left(\frac{\pi}{6} D_d^3\right)\rho_g h_{fg} \tag{2}$$

where N'' is the bubble nucleation site density, f is the bubble departure frequency, D_d is the bubble departure diameter, ρ_g is the gas density, and h_{fg} is the latent heat of evaporation.

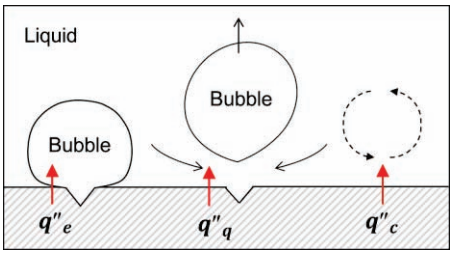

Figure 1. Conceptual description of the wall heat-flux partitioning model.

The quenching heat flux, $q_q^{"}$, is the heat flux required to reform the thermal boundary layer and is a transient conduction heat flux:

$$q_q^{"} = \left(\frac{2}{\sqrt{\pi}} \sqrt{t_w k_l \rho_l C_{pl}} f \right) A_{2f} \left(T_w - T_l \right) \tag{3}$$

where t_w is the bubble wait time, k_l is the conductivity of the liquid, C_{pl} is the specific heat of the liquid, T_w is the wall temperature, and T_l is the bulk liquid temperature. The quenching heat flux occurs in the bubble influence area, called to the two-phase area ratio (A_{2f}).

The convective heat flux, $q_c^{"}$, is the heat flux transferred to the liquid phase outside the bubble influence area as follows:

$$q_c^{"} = h_c A_{1f} \left(T_w - T_l \right) \tag{4}$$

where A_{1f} is the ratio of the single-phase area to the total area.

The equations for the partitioned heat fluxes consist of the wall temperature, fluid properties, and bubble parameters. Table I shows the basic sub-models [6-8] for the bubble parameters used in commercial CFD code [9]. Note the absence of dependency on the flow velocity and surface orientation, as shown in Table I; the bubble parameters are determined only by the wall temperature. Several efforts have been made to evolve the mechanistic models for subcooled flow boiling on a vertical wall, focusing on practical applications such as rod bundles in a nuclear reactor vessel [10–11]. However, the effects of surface orientation on heat partitioning model have not yet been quantified.

Table I. Default correlation for bubble parameter used in commercial CFD code [9]

Parameter	Correlation	Unit	Reference
Nucleation site density	$N^{"} = \left[185 \left(T_w - T_{sat} \right) \right]^{1.805}$	#/m^2	Lemmart and Chawla [6]
Bubble departure diameter	$D_d = 0.6 \cdot 10^{-3} e^{-\frac{T_w - T_l}{45}}$	m	Tolubinski and Kostanchuk [7]
Bubble departure frequency	$f = \sqrt{\frac{4g(\rho_l - \rho_g)}{3 D_d \rho_l}}$	s^{-1}	Cole [8]
Bubble wait time	$t_w = \frac{0.8}{f}$	s	Tolubinski and Kostanchuk [7]
Convective heat transfer coef.	$h_{c,l} = \frac{\rho_l C_{p,l} u_\tau}{T^+}$	W/m^{2}K	
Single-phase area ratio	$A_{1f} = 1 - A_{2f}$	-	
Two-phase area ratio	$A_{2f} = N^{"} \frac{\pi D_b^2}{4} K$	-	
Bubble influence factor	K=4	-	

3. EXPERIMENTAL

3.1. Measurement method for the bubble parameters

An integrated visible and infrared optical method was used to simultaneously gather experimental high-resolution data for the local bubble parameters. Three measurement techniques, total reflection (TR), infrared thermometry (IR), and side visualization, were temporally and spatially synchronized, as shown in Fig. 2. A detailed description of the method can be found in our previous paper [12].

Since the TR technique detects the distribution of the liquid and vapor phases on a boiling surface, several bubble parameters can be measured, as such the nucleation site density, bubble departure frequency, and bubble wait time, as seen in Fig. 2. The nucleation site was marked with the total reflection images as seen in Fig. 2(a). The bubble departure frequency was straightforward to measure using total reflection images. Figure 2(d) shows history of light intensity for a specific nucleation site of interest for one second. The intensity is 1 when it is dry because of a boiling bubble, and 0 when wetted. The change from 1 to 0 indicates departure of a bubble from the wall and the time for zero intensity corresponds to the wait time. Therefore, the bubble departure frequency and wait time was measured by counting the change per second. Since the IR technique measures the surface temperature distribution on the boiling surface, it provides the average surface temperature. The nucleation site density can be obtained from thermal footprints in the IR images, as seen in Fig. 2(b) [13]. Finally, the side visualization images can be used to observe the bubble behavior, allowing to measure the bubble departure diameter, as seen in Fig. 2(c).

As for the non-isolated region, only isolated bubble were collected, as seen in Fig. 3, and then we measured bubble departure diameter, bubble departure frequency and wait time with the same principle as seen in Fig. 2..

The maximum measurement errors are estimated at 0.12 mm for bubble departure diameter and 0.4 ms for wait time. Since the nucleation sites are manually tracked within TR image, bubbles smaller than a camera pixel (<30 μm) and faster than the camera frame rate (<0.2 ms) could be missed. The bubbles may be too small or fast to have much effect on the total heat transfer, so these are negligible.

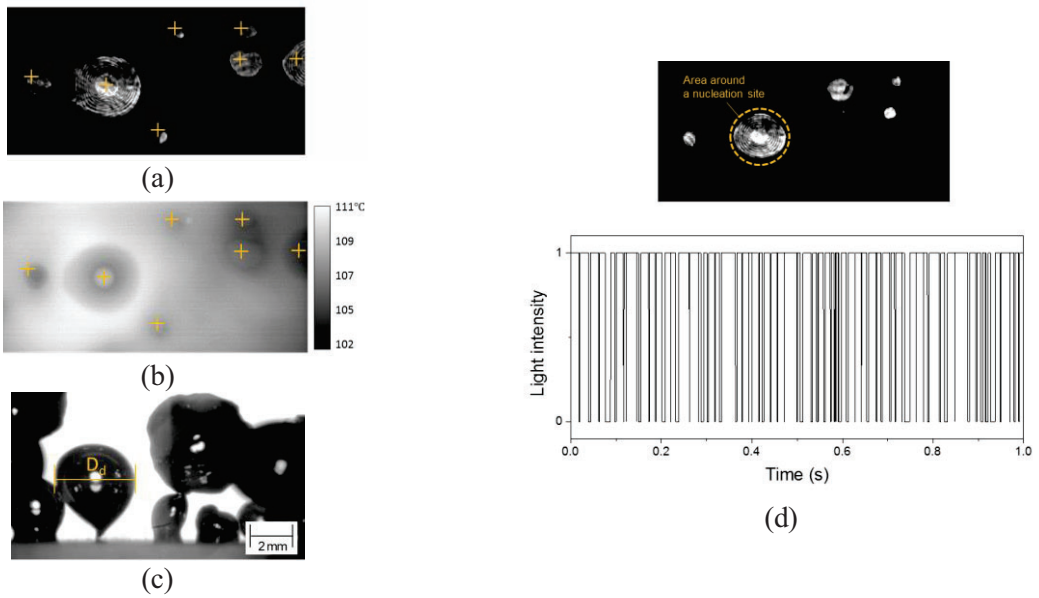

Figure 2. Measurement principle of bubble parameters such as nucleation site density, bubble departure diameter, bubble departure frequency and wait time.

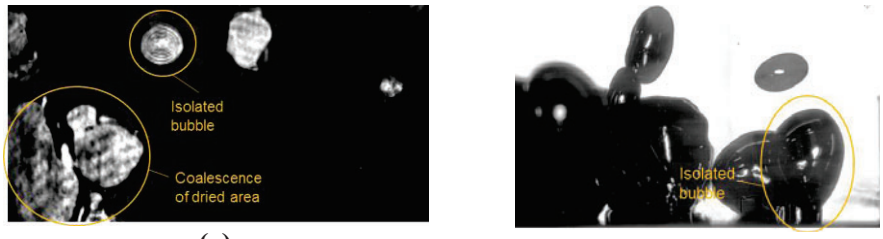

(a) (b)

Figure 3. Measurement principle of bubble parameters such as nucleation site density, bubble departure diameter, bubble departure frequency and wait time.

3.2. Experimental apparatus

The experimental setup was designed to examine the nucleate pool boiling heat transfer, as seen in Fig. 4(a). The facility consisted of test section, optic devices and the rotatable optical table. The test section consisted of a boiling pool with a test sample as 700-nm-thick ITO film heater on the sapphire disk in 10 mm thickness, immersion heaters and T-type thermocouple to maintain and measure the liquid temperature, respectively, and a reflux condenser. The electro-conductive ITO film had a sheet resistance of 10 Ohm/sq and the static contact angle of a water droplet on the film was 67°. The optic devices for the visible and infrared optical method were composed with the two high-speed-cameras, an infrared camera, He-Ne laser, and optical devices such as beam expander, reflection mirrors and interference filter. The optical table for array of test section and optical devices was designed to be rotated for varying orientation from the upward-facing horizontal to down-facing horizontal at 15 degree intervals, as seen in Fig. 4(b).

3.3. Input heat flux and temperature uncertainties

The input heat flux was calculated by the voltage and current measured with data acquisition system (DAS) and the active heater area. The uncertainties are 0.1% in the voltage, 1.7% in the current, and 1.4% in the heater area. As the experiment data presented in this paper were obtained for four heat fluxes (103, 146, 270 and 469 kW/m^2), the measurement uncertainty for the input heat flux was less than 2.2%.

ITO film has the advantage of being opaque in the infrared range, unlike a sapphire substrate, which is transparent to infrared light. This ensures that all temperature measurements are made on the back (bottom) of the ITO layer. The thinness of the ITO heater, 700 nm, ensured that the infrared radiation measured on its bottom surface was an accurate representation of the actual temperature on the top of the heater surface [13]. The calculated maximum error in the temperature measurement due to the accumulated radiation from the sapphire substrate was 1.5°C which is bias error. A T-type thermocouple was used to measure temperature of the ITO layer for the calibration. This introduced the uncertainty of 0.5°C. Hence, the uncertainty of the temperature measurements was approximately 2°C.

4. RESULTS AND DISCUSSION

The experimental data presented in this paper were obtained for nucleate boiling of saturated water in a pool under atmospheric pressure by means of the integrated visible and infrared optical method.

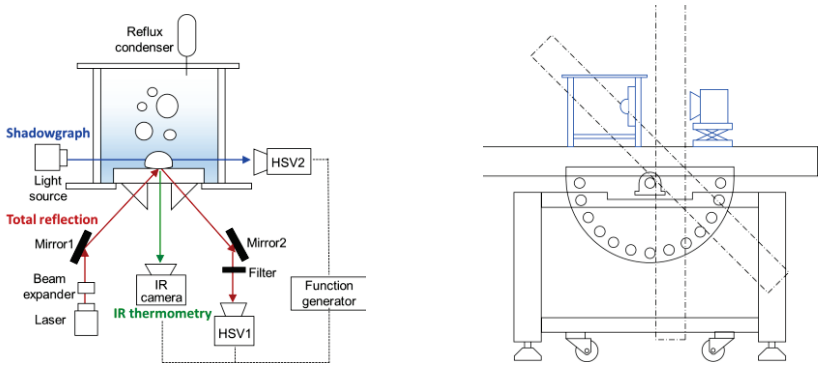

Figure 4. (a) Schematic diagram of the experimental setup (b) Schematic of the rotatable optical table.

4.1. Effects of surface orientation on the boiling phenomena

Figure 5 shows the experiment results of boiling curve on different orientation in low heat flux nucleate boiling region (< 500 kW/m^2). The heat flux generally increases with increasing the orientation angle, but it is much the same at the orientation angle of 0°, 30°. The obtained result shows fairly good agreement in trend with the experimental results of previous studies [1-4] in that heat transfer coefficient increased when the surface inclined from upward facing horizontal to vertical in the low heat flux nucleate boiling region. Therefore, the experiment results show the general trend of boiling curve with regard to surface orientation. Note that the RPI model predicts low heat flux at given wall superheat compared to experiment results as shown in Fig. 5.

In order to focus on the effects of surface orientation, we analyzed the experiment results at constant surface temperature since the sub-models for wall heat flux partitioning are determined only by the wall temperature as given in Table I. The given temperature is 107.5°C at the orientation angle of 0° (upward-facing horizontal), 30°, 60°, and 90° (vertical). In present study, the temperature distribution on boiling surface was measured using infrared thermometry technique and the average surface temperature to heated surface could be displayed during the boiling test. It enabled the average surface temperature to be controlled in real time. The applied heat flux to maintain the same average wall superheat were noticeably different with respect to the orientation: the applied heat fluxes were 103, 146, 270, and 469 kW/m^2 for orientation angles of 0, 30, 60, and 90°, respectively.

Experiment results of bubble shape and liquid-vapor phase and temperature distributions on the wall with the effect of the wall orientation are presented in Table II. The spatial and temporal resolutions were 45 μm and 2 ms for the temperature measurement images and 30 μm and 0.2 ms for the liquid-vapor phase detection and bubble shape images. It is observed that the dynamic of bubbles and heat transfer on the heated surface depend on the surface orientation. There are more massive interactions of bubbles when the surface inclined from upward facing horizontal to vertical. In addition, there is a difference in heat transfer characteristic regarding surface orientation, as seen in temperature distributions of Table II. At the surface orientation of 0° and 30°, the thermal pattern by bubble is symmetric with respect to the center of bubble, while at the surface orientation of 60° and 90° the thermal patterns were biased toward the upper side of the heater because the bubble traveled along the inclined wall. Note that the left-hand side for temperature distributions corresponds to the upside of heater. However, these different physical characteristics such as bubble sliding and merging are not incorporated in the RPI model, even though they may play a significant role in the increase of heat transfer coefficient. Therefore, it is necessary to examine the effects of the surface orientation. A quantitative analysis for that is given in the following section.

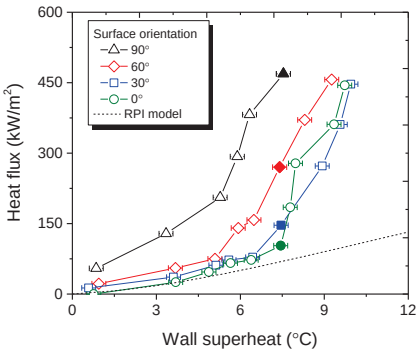

Figure 5. Effect of surface orientation on boiling curve (the first and last points do not represent ONB or CHF).

Table II. Visualization results for different surface orientations at a wall superheat of 7.5°C.

Wall superheat	7.5°C			
Orientation	0°	30°	60°	90°
Avg. heat flux	103 kW/m^2	146 kW/m^2	270 kW/m^2	469 kW/m^2
Bubble dynamics	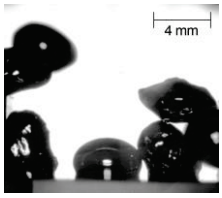	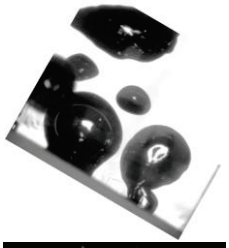	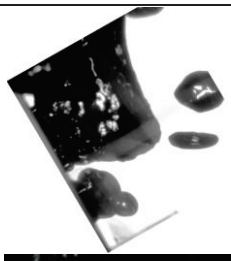	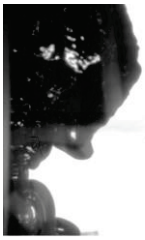
Phase distribution Gas Liquid	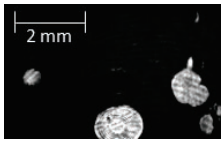		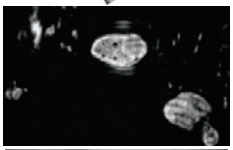	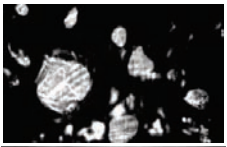
Temperature distribution 100 111 °C	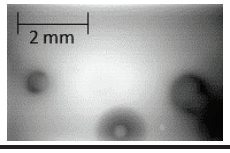	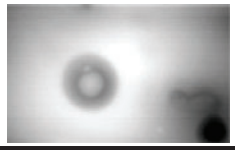	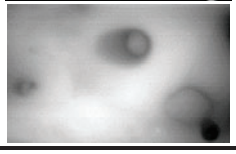	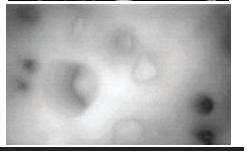

4.2. Effects of surface orientation on the bubble parameters

In this section, we examine the effects of surface orientation on the bubble parameters and then compare them with various bubble parameter correlations, including the basic sub-models used in the RPI model listed in Table I. Figures 6–9 present the measured data including the nucleation site density, bubble departure diameter, bubble departure frequency and wait time as functions of the surface orientation angle, along with correlations. The measured parameters shows averaged value. The sample number of bubbles for each parameter is summarized in Table III. The experimental data and predicted data showed different tendencies at given constant surface temperature of 107.5°C. A detailed discussion of each bubble parameter with regard to the surface orientation angle is given in the following paragraphs.

4.2.1. Nucleation site density

Figure 6 shows the effects of the surface orientation on the nucleation site density for the measured and predicted data. In the experiments, the nucleation site density increased with the orientation angle, and a drastic increase was observed for the vertical surface. Chang and You [5] reported the same trend. As the surface orientation increases, the superheated boundary layer becomes increasingly thick on the upper side of the heater, which leads to more activated nucleation sites. Evidence of this can be seen in the nucleation site density distributions shown in Fig. 10. The nucleation site density was confirmed to be greater on the upper surface than on the lower surface. However, the data predicted by the basic and alternative sub-models remained constant, as seen in Fig. 6.

4.2.2. Bubble departure diameter

In the RPI model, the bubble departure diameter is limited to an isolated bubble [5]. An increase in the nucleation site density decreases the spacing between adjacent bubbles, and increases the amount of mutual bubble interactions such as bubble merging. In addition, a bubble sliding along an inclined wall that meets a bubble on the upper side of the heater forms a merged bubble. Thus, isolated bubbles become rarer as the surface orientation angle increases, as shown in Table II, and isolated bubbles cannot represent the actual physical phenomena occurring at an inclined wall. Therefore, we measured the bubble departure diameter for isolated bubbles and all bubbles, including merged bubbles, and compared the difference between the values.

In the measured data shown in Fig. 7, the two average bubble departure diameters had different tendencies with respect to the surface orientation: when the surface was inclined from 0 to 90º, the bubble departure diameter for the isolated bubbles decreased, whereas the average bubble departure diameter for both the isolated and merged bubbles increased. As the surface orientation angle increased, more turbulence is generated in the thermal boundary layer due to the active bubble behavior, which could make it easier for isolated bubbles to depart at earlier stages of their growth, resulting in a decrease in the bubble departure diameter for isolated bubbles [13]. However, bubble merging is more active due to bubble sliding and the increased nucleation site density, which increases the bubble departure diameter for merged bubbles [14]. The bubble departure diameter correlations predict constant values, regardless of the surface orientation angle. An increased bubble departure diameter leads to increased evaporative and quenching heat fluxes, and vice versa. Therefore, the use of the bubble departure diameter for isolated bubbles decreases the total wall heat flux with increasing surface orientation angle, which is opposite to the trend observed in the measured data; this indicated an increase in the total wall heat flux from 103 to 469 kW/m^2 as the orientation angle increased from 0 to 90°.

4.2.3. Bubble departure frequency

As shown in Fig. 8(a), the measured data indicate that the bubble departure frequency for isolated bubbles increases with the surface orientation angle. This is because the turbulent motion enhanced by the bubble interactions causes the growing bubble to depart prematurely from the wall. Isolated bubbles are generally observed to be absorbed into the merged bubble, which also causes the bubbles to depart early from the wall.

In Fig. 8(a), the data predicted using the basic sub-models are constant. Tolubinski and Kostanchuk's basic sub-model [7] for the bubble departure diameter predicts a smaller value than the measured bubble departure diameter, as shown in Fig. 7. Cole's basic sub-model [8] for the bubble departure frequency gives predictions that are inversely proportional to the bubble departure diameter; hence, the predicted bubble departure frequency is higher than the experiment data. When we calculated the bubble departure frequency using Cole's [8] model with our measured bubble departure diameter for isolated bubbles, the results were in good agreement with the experimentally observed trends shown in Fig. 8(a).

Figure 8(b) shows the measured bubble departure frequency as a function of bubble departure diameter, along with predictions using the basic and alternative sub-models. Good agreement existed in terms of the order of magnitude and trends of the measured and predicted data. In particular, Zuber's model [15] corresponded well with the measured data, which indicates that the sub-models reflect the dependency on the bubble departure diameter. Directly measuring the bubble departure frequencies and wait times for merged bubbles is impossible since the merged bubbles are formed irregularly. Therefore, we predicted the bubble departure frequency using Zuber's [15] model with the measured bubble departure diameter for merged bubbles, as shown in Fig. 8(b).

4.2.4. Bubble wait time

The measured wait time for isolated bubbles decreased with increasing surface orientation angle, as shown in Fig. 9(a). This is in agreement with our bubble departure frequency observations since the wait time is inversely proportional to the departure frequency according to the following definition:

$$f = \frac{1}{t_w + t_g} \tag{5}$$

The data predicted using the basic sub-models were constant, regardless of the surface orientation, while the data predicted using the measured bubble departure frequency for isolated bubbles agreed well with the measured wait times. Therefore, Tolubinski and Kostanchuk's model [7], which is the basic sub-model for bubble wait time, reflects the dependency on the bubble departure frequency well, as shown in Fig. 9(b). Hence, we predicted the bubble wait time for merged bubbles with Tolubinski and Kostanchuk's [7] model using the bubble departure frequency obtained in the previous section.

Table III. Sample number of bubble for each parameter

Orientation (˚)	Number of nucleation site	Sampling number of bubbles (nucleation sites)					Sampling time (s)
		Departure frequency	Wait time	Departure diameter		Sliding length	
				Isolated	Merged		
0	8	342(8)	342(8)	44(4)	21	44(4)	1
30	9	399(8)	399(8)	42(4)	34	42(4)	
60	13	542(8)	542(8)	26(4)	16	26(4)	
90	31	1371(18)	1371(18)	4(2)	8	4(2)	

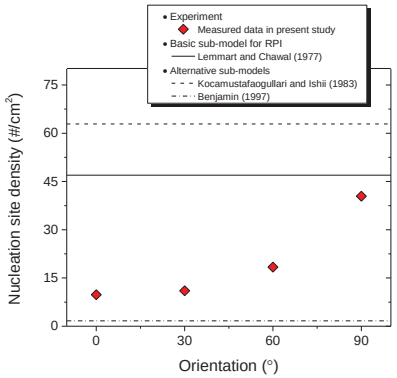

Figure 6. Nucleation site density as a function of surface orientation (T_{wall}=107.5°C).

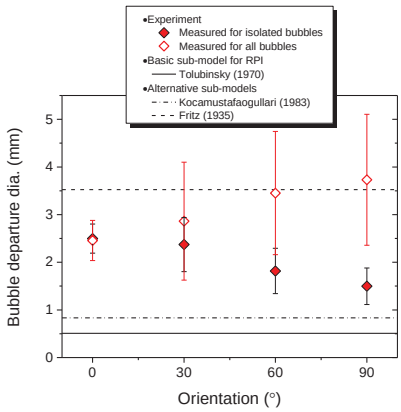

Figure 7. Bubble departure diameter as a function of surface orientation (T_{wall}=107.5°C).

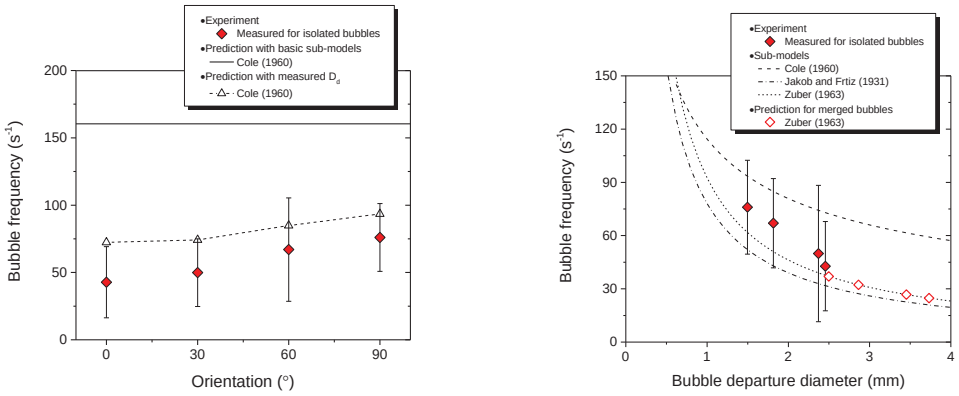

(a) (b)

Figure 8. Bubble departure frequency as a function of (a) surface orientation and (b) bubble departure diameter (T_{wall}=107.5°C).

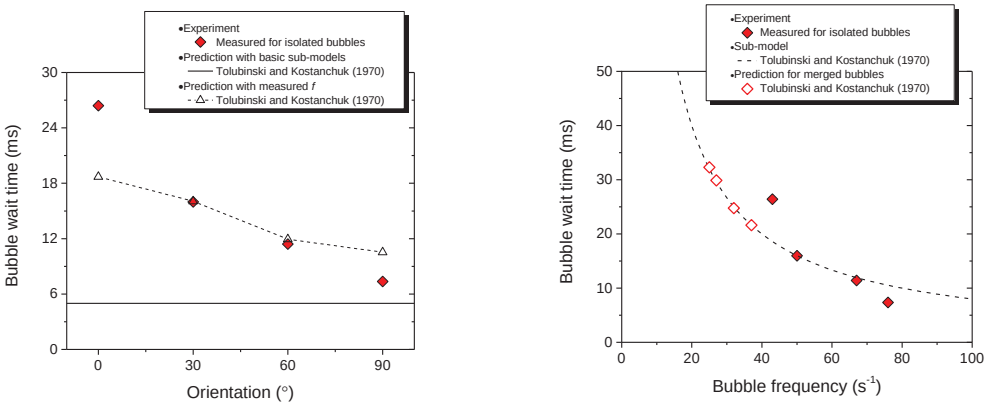

(a) (b)

Figure 9. Bubble wait time as a function of (a) surface orientation and (b) bubble departure frequency (T_{wall}=107.5°C).

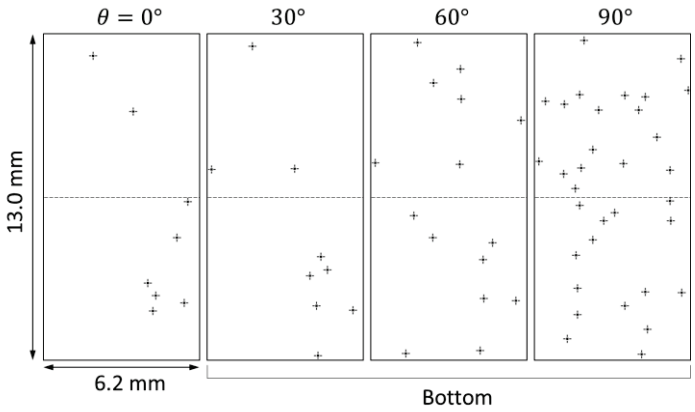

Figure 10. Distributions of nucleation sites on the inclined wall at 0, 30, 60, and 90° (T_{wall}=107.5°C).

4.3. Effects of surface orientation on the bubble influence area

The bubble influence area is the region where transient conduction takes place. The ratio of the bubble influence area in a wall heat-flux partitioning model is as follows:

$$A_{2f} = N'' \frac{\pi D_b^2}{4} K \tag{6}$$

Prior to discussing the effect of the surface orientation on the bubble influence area, we must first determine the physical meaning of the bubble influence factor K. Han and Griffith [16] proposed that the effective diameter of the influence area is twice the bubble departure diameter (D_{inf}= $2D_b$) without any experimental evidence. Since then, a bubble influence factor of 4 has been commonly used to evaluate the bubble influence area in commercial CFD codes [9], which means that the effective diameter of the bubble influence area is twice the bubble departure diameter. However, some researchers have suggested lower values for the empirical bubble influence area for an isolated bubble (D_{inf}~ $0.5D_b$) [12, 17, 18]. In our earlier study [18], we ascertained it is best consistent with experimentally measured data when the K is 0.25. We conjugated therefore the K of 0.25 in the data reported here. But more studies are necessary to determine the general value of K with various fluids under different subcooling and pressure conditions.

In addition to the bubble parameters discussed in previous section, we considered the effect of bubble sliding on the inclined surface on the bubble influence area. The ratio of bubble influence area is just for stationary bubble in Eq (6). The experiment results obviously show the bubble travelling along with wall have each bubble sliding distance with the surface orientation. Therefore, the influence area with sliding bubble should include both area for the stationary bubble and sliding bubble. The ratio of bubble influence area including both stationary and sliding bubble can be expressed as,

$$A_{2f} = N'' K \left(l_s D + \frac{\pi D^2}{4} \right) \tag{7}$$

where l_s is the bubble sliding distance and D is the average bubble diameter. In our experiment, it is found that the average values for the sliding length were 2.1 mm, 3.0 mm and 6.4 mm for orientation angle of 30°, 60°, and 90°, respectively. In this study, the effect of bubble sliding and merging on the ratio of the bubble influenced and total wall heat flux was considered.

4.4. Effects of surface orientation on the wall heat-flux partitioning

In the preceding section, the effects of the wall orientation on the bubble parameters and bubble influence area were examined in detail. These are sub-parameters to predict the partitioned heat fluxes (i.e. evaporation, transient conduction, and convection) and total wall heat flux. In this section, we focus on the effects of surface orientation on heat transfer on the wall at given wall superheat of 7.5°C and discuss the physical mechanism accompanying the change of heat transfer performance.

First, we compared the total heat flux between experimentally measured data and prediction data with basic sub-models. Fig. 11 (a) shows the total wall heat flux for the experiment and RPI model. In the experiment, the total wall heat flux increases with surface orientation. The increase can be attributed to surface orientation since the each constitutive bubble parameter is strongly influenced by surface orientation, as given in Fig. 6-9. On the other hand, the prediction data shows almost constant value regardless of surface orientation. There was a slight increase because the convection heat transfer coefficient increases with surface orientation. However, it was very small increase compared to measured heat flux. It is necessary to examine in detail what physical mechanism leads to the change of heat transfer performance with respect to surface orientation in experiment. It is discussed in following paragraphs.

Fig. 11 (b) shows the total wall heat flux calculated by RPI model with bubble parameters from experiment, such as nucleation site density, bubble departure diameter, bubble departure frequency, and bubble wait time. The total heat flux predicted with bubble parameters for isolated bubbles was almost constant regardless of surface orientation, whereas the total heat flux predicted for merged bubbles remarkably increased with the surface orientation. The trend is similar in the measured data. As mentioned in Section 4.2.2, only consideration of isolated bubbles cannot represent the actual physical phenomena, since the merged bubbles are more prevalent as increasing the surface orientation. It is fair that the prediction data for merged bubbles were in good agreement with the experimentally measured data. Therefore, it is important to consider the merged bubbles for wall heat transfer. Especially, the bubble departure diameter for merged bubbles is major factor to dominate the boiling heat transfer. On the other hand, considering the effect of bubble sliding, there was very little change in the total wall heat flux according to surface orientation, even though the ratio of bubble influence area ratio noticeably increases, as seen in Fig. 11 (b). It indicates that the effect of bubble sliding on the total wall heat flux is negligible.

Figure 12 shows the heat flux partitioning for RPI prediction with the measured data for merged bubbles with regard to surface orientation. As the surface orientation increased, the evaporation heat flux drastically increased. The quenching heat flux also increased, but it is small compared to increase of the total heat flux and the convection heat flux was almost zero. It indicates that drastic increase of total wall heat flux was attributed to the increase of evaporation heat flux. Therefore, we can conclude that the evaporation is dominant contributor for heat flux that is greater than 65 % of total heat flux in all surface orientation cases during saturated pool boiling of water at atmospheric pressure. It is consistent with the experimental results reported in previous study [19]. Graham and Hendricks [19] examined the relative contribution of each heat flux according to the averaged heat flux, and found that the evaporation became the dominant heat transfer mechanism for subcooled water as the averaged heat flux increases.

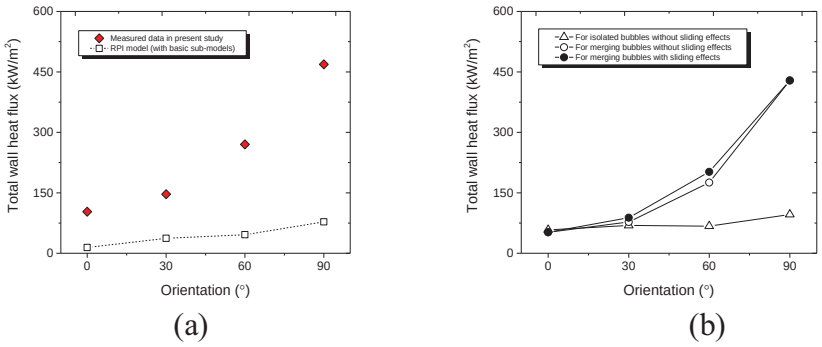

Figure 11. Total wall heat flux as a function of surface orientation: (a) comparison between experiments and the RPI model and (b) data predicted by the RPI model using bubble parameters obtained from the experiments (T_{wall}=107.5°C).

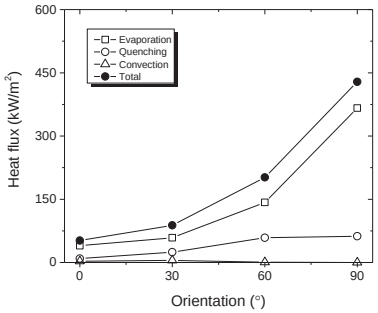

Figure 12. Heat flux partitioning for the RPI predictions using measured data for merged bubbles as a function of surface orientation (T_{wall}=107.5°C).

5. CONCLUSIONS

We experimentally examined the effects of surface orientation on the wall heat-flux partitioning model for pool boiling of saturated water at atmospheric pressure through the simultaneous measurement of bubble parameters. The measured data were compared with data predicted by the RPI model for various surface orientation at a constant surface temperature of 107.5°C. Our findings can be summarized as follows.

- The heat transfer performance significantly increased as increasing the surface orientation from upward-facing horizontal (0°) to vertical (90°) in low heat flux nucleate boiling region (<500 kW/m^2). This was due to the mechanisms at inclined wall, such as bubble sliding and merging.
- The experiment and the prediction model showed different tendencies with respect to wall orientation at the constant surface temperature of 107.5°C: as the angle of surface orientation changes from 0° to 90°, the nucleation site density, average bubble departure diameter, and bubble departure frequency increased, and the bubble wait time decreased, while the basic sub-model of RPI model predicted almost constant values for the corresponding parameters regardless of the wall orientation angle because of the constant wall superheat.
- There was a big difference in total wall heat flux between measured data and prediction data by RPI model with respect to surface orientation. The measured total heat flux remarkably increased with orientation angle, while the RPI model predicted almost constant. The main cause of that was the effect of bubble merging, whereas the effect of bubble sliding was negligible.
- The evaporation was the dominant contributor for heat flux that is greater than 65 % of total heat flux with surface orientation of 0, 30, 60, 90°.

ACKNOWLEDGMENTS

This work was supported by the Nuclear Power Core Technology Development Program of the Korea Institute of Energy Technology Evaluation and Planning (KETEP), and granted financial resources by the Ministry of Trade, Industry & Energy, Republic of Korea (No. 20131520000090).

REFERENCES

1. B.D. Marcus and D. Dropkin, "The effect of surface configuration on nucleate boiling heat transfer," *International Journal of Heat and Mass Transfer*, **6**, pp. 863-867 (1963).
2. A.T. Storr, "The effect of heating surface geometry and orientation on nucleate moiling of subcooled water," M.S. Thesis, Washington University, Sever Institute of Technology (1958).
3. K. Nishikawa, Y. Fuijta, S. Uchida, H. Ohta, "Effect of surface configuration on nucleate boiling heat transfer," *International Journal of Heat and Mass Transfer*, **27**, pp. 1559-1571 (1983).
4. J.Y. Chang and S.M. You, "Heater orientation effects on pool boiling of micro-porous-enhanced surfaces in saturated FC-72," *Journal of Heat and Mass Transfer,* **118**, pp. 937-943 (1996).
5. N. Kurul and M.Z. Podowski, "Multidimentional effects in forced convection sub-cooled boiling," *Proceedings of 9th International Heat Transfer Conference*, Jerusalem, Israel, August 21–26 (1990).
6. M. Lemmart and L.M. Chawla, "Influence of flow velocity on surface boiling heat transfer coefficient," Heat Transfer in Boiling, E. Hahne and U. Grigull, Eds., Academic Press and Hemisphere, New York, USA, (1977).
7. V.I. Tolubinsky and D.M. Kostanchuk, "Vapour bubbles growth rate and heat transfer intensity at subcooled water boiling heat transfer," *Proceedings of 4th International Heat Transfer Conference*, Paris, **5**, Paper No. B-2.8 (1970).
8. R. Cole, "Photographic study of boiling in region of critical heat flux," AIChE Journal **6**, pp. 533-542 (1960).
9. ANSYS CFX-Solver Modeling Guide, UK (2013).
10. N. Basu, G.R. Warrier and V. K. Dhir, "Wall heat-flux partitioning during subcooled flow boiling: Part I – Model development," *Journal of Heat Transfer,* **127**, pp. 131-140 (2005).
11. B. Bae, "Development of CFD code for subcooled boiling two-phase flow with modeling the interfacial area transport equation," Ph.D. Dissertation, Seoul National University (2008).
12. S. Jung, H. Kim, "An experimental method to simultaneously measure the dynamics and heat transfer associated with a single bubble during nucleate boiling on a horizontal surface," *International Journal of Heat and Mass Transfer*, **73**, pp. 365-375 (2014).
13. C.D. Gerardi, "Investigation of the pool boiling heat transfer enhancement of nano-engineered fluids by means of high-speed infrared thermography," Ph.D. Dissertation, Massachusetts Institute of Technology (2009).
14. N.I. Kolev, "The influence of mutual bubble interaction on the bubble departure diameter," *Experimental Thermal and Fluid Science*, **8**, pp. 167–174 (1994).
15. N. Zuber, "Nucleate boiling – The region of isolated bubbles – Similarity with natural convection," *International Journal of Heat and Mass Transfer*, **6**, pp. 53-65 (1963).
16. C. Han and P. Griffith, "The mechanism of heat transfer in nucleate pool boiling – Part II: The heat flux-temperature difference relation," *International Journal of Heat and Mass Transfer*, **8**, pp. 905-614 (1965).
17. S. Moghaddam, and K. Kiger, "Physical mechanisms of heat transfer during single bubble nucleate boiling of FC-72 under saturation conditions – I. Experimental investigation," *International Journal of Heat and Mass Transfer*, **52**, pp. 1284–1294 (2009).
18. J. Song, J. Park, S. Jung and H. Kim, "Experimental study on heat-flux partitioning in subcooled nucleate boiling on vertical wall," *Transactions of the Korean Society of Mechanical Engineers B*, **38**, pp. 464-474 (2014) (in Korean).
19. R.W. Graham, R.C. Hendricks, "Assessment of convection, conduction and evaporation in nucleate boiling," NASA TND-3943, National Technical Information Service, Springfield, VA, 5 (1967).